

TECHNICAL REPORT BRL-TR-2926

BRL

1938 - Serving the Army for Fifty Years - 1988

ANALYSIS OF AN INVERSE RAILGUN
WITH A RAILGUN LOAD

AD-A196 619

DTIC
ELECTE
JUL 22 1988
S & D D

JOHN D. POWELL
KEITH A. JAMISON

JULY 1988

APPROVED FOR PUBLIC RELEASE; DISTRIBUTION UNLIMITED.

U.S. ARMY LABORATORY COMMAND

BALLISTIC RESEARCH LABORATORY
ABERDEEN PROVING GROUND, MARYLAND

DESTRUCTION NOTICE

Destroy this report when it is no longer needed. DO NOT return it to the originator.

Additional copies of this report may be obtained from the National Technical Information Service, U.S. Department of Commerce, Springfield, VA 22161.

The findings of this report are not to be construed as an official Department of the Army position, unless so designated by other authorized documents.

The use of trade names or manufacturers' names in this report does not constitute indorsement of any commercial product.

REPORT DOCUMENTATION PAGE

1a. REPORT SECURITY CLASSIFICATION Unclassified				1b. RESTRICTIVE MARKINGS			
2a. SECURITY CLASSIFICATION AUTHORITY				3. DISTRIBUTION / AVAILABILITY OF REPORT			
2b. DECLASSIFICATION / DOWNGRADING SCHEDULE							
4. PERFORMING ORGANIZATION REPORT NUMBER(S) BRL-TR-2926				5. MONITORING ORGANIZATION REPORT NUMBER(S)			
6a. NAME OF PERFORMING ORGANIZATION US Army Ballistic Research Laboratory		6b. OFFICE SYMBOL (If applicable) SLCBR-TB-EP		7a. NAME OF MONITORING ORGANIZATION			
6c. ADDRESS (City, State, and ZIP Code) Aberdeen Proving Ground, MD 21005-5066				7b. ADDRESS (City, State, and ZIP Code)			
8a. NAME OF FUNDING / SPONSORING ORGANIZATION US Army Ballistic Research Laboratory		8b. OFFICE SYMBOL (If applicable) SLCBR-D		9. PROCUREMENT INSTRUMENT IDENTIFICATION NUMBER			
8c. ADDRESS (City, State, and ZIP Code) Aberdeen Proving Ground, MD 21005-5066				10. SOURCE OF FUNDING NUMBERS			
				PROGRAM ELEMENT NO. 61101A	PROJECT NO. A91A	TASK NO. 00	WORK UNIT ACCESSION NO. 001AJ
11. TITLE (Include Security Classification) (U) Analysis of an Inverse Railgun with a Railgun Load							
12. PERSONAL AUTHOR(S) John D. Powell and Keith A. Jamison							
13a. TYPE OF REPORT		13b. TIME COVERED FROM _____ TO _____		14. DATE OF REPORT (Year, Month, Day)		15. PAGE COUNT	
16. SUPPLEMENTARY NOTATION							
17. COSATI CODES			18. SUBJECT TERMS (Continue on reverse if necessary and identify by block number) inverse railgun, railgun, electromagnetic propulsion, electromagnetic gun				
FIELD	GROUP	SUB-GROUP					
20	03						
19. ABSTRACT (Continue on reverse if necessary and identify by block number) (ldk) <p>→ A model is presented to analyze theoretically an inverse railgun used as a power supply for a railgun. The governing equations are developed and it is shown that they possess an exact analytic solution in the limit that resistive effects can be neglected. These limiting-case solutions are used to study qualitatively the behavior of the inverse railgun in this configuration. More general numerical solutions, which account approximately for resistive effects, are then undertaken and discussed in some detail. Emphasis is placed on determining design parameters which optimize energy transfer between the two devices. The analysis suggests that the railgun, unlike most other loads, can be powered effectively with an inverse railgun.</p>							
20. DISTRIBUTION / AVAILABILITY OF ABSTRACT <input checked="" type="checkbox"/> UNCLASSIFIED/UNLIMITED <input type="checkbox"/> SAME AS RPT. <input type="checkbox"/> DTIC USERS				21. ABSTRACT SECURITY CLASSIFICATION UNCLASSIFIED			
22a. NAME OF RESPONSIBLE INDIVIDUAL John D. Powell				22b. TELEPHONE (Include Area Code) (301) 278-5783		22c. OFFICE SYMBOL SLCBR-TB-EP	

TABLE OF CONTENTS

	<u>Page</u>
LIST OF FIGURES	v
I. INTRODUCTION	1
II. MODEL AND GOVERNING EQUATIONS	2
III. SOLUTION FOR NO RESISTANCE	6
IV. EFFECTS OF RESISTANCE	14
A. Analysis	14
B. Numerical Technique	18
C. Results	19
V. SUMMARY AND CONCLUSIONS	23
REFERENCES	27
LIST OF MOST COMMONLY USED SYMBOLS	29
APPENDIX	31
DISTRIBUTION LIST	35



Accession For	
NTIS CRA&I	<input checked="" type="checkbox"/>
DTIC TAB	<input type="checkbox"/>
Unannounced	<input type="checkbox"/>
Justification	
By	
Distribution	
Availability Codes	
Dist	Availability Codes
A-1	

LIST OF FIGURES

<u>Figure</u>	<u>Page</u>
1 Schematic diagram of model and conceptual drawing of IRG-RG configuration	3
2 Performance of IRG with no resistance ($\alpha = 0.1, \gamma = 14.0, \beta = 3.8$)	9
3 Performance of IRG with no resistance ($\alpha = 0.01, \gamma = 14.0, \beta = 12.0$)	10
4 Performance of IRG with no resistance ($\alpha = 0.01, \gamma = 7.0, \beta = 10.0$)	12
5 Effect of varying β on maximum velocity achieved by railgun armature	13
6 Performance of IRG with resistance ($\alpha = 0.1, \gamma = 14.0, \beta = 6.3$).	20
7 Potential per unit length along IRG rails	22
8 Performance of IRG with resistance ($\alpha = 0.01, \gamma = 7.0, \beta = 15.2$)	24
9 Performance of IRG with resistance ($\alpha = 0.005, \gamma = 7.0, \beta = 22.5$)	25

I. INTRODUCTION

In recent years there has been considerable emphasis on the research and development of various electromagnetic-propulsion devices. In addition to technological problems associated with the devices themselves, it has long been recognized that the electrical-power requirements necessary for driving these accelerators would be quite severe. In particular, it is necessary to develop a power source which is reusable, which is lightweight, and which is capable of delivering megajoules of energy on a time scale of a few milliseconds. Various types of power supplies are now in common use, but all have fairly significant disadvantages. A brief summary of some of the more common sources and their limitations has been presented elsewhere.¹

One type of power supply alluded to frequently in the past, but which until recently has not received much detailed study, is the inverse railgun (IRG). The basic concept upon which the IRG works is quite straightforward. It is constructed as a railgun but with some load resistance and/or inductance connected across the muzzle and with a seed current initially in the circuit. Rather than the current providing the principal force that drives the armature away from the flux entrained in the bore, however, the armature is driven toward the flux by an external force. If it proceeds rapidly forward the current rises and mechanical energy is converted into electrical energy. Basically three factors must be present for the IRG to operate as an efficient electrical generator: First, the external force which drives the armature must be sufficient to cause current gain in the circuit. If the velocity is too low the energy will be dissipated resistively before current gain can occur. Second, the armature must be completely decelerated; otherwise, there will be inefficient conversion of kinetic to electrical energy. Finally, the electrical energy must be extracted from the IRG in a timely manner before the armature can be accelerated backwards by the magnetic forces in the circuit.

In fairly recent work, Marshall¹ has considered using an IRG to charge an inductor which was in turn to be used for earth-to-space rail-launch applications. He concluded that the device was worthy of further study. Later, Benford, Kares, Brooks and Goldman² investigated the possibility of using IRGs to charge inductive stores positioned along a segmented railgun. At least for some applications IRGs were found to be more practical for this use than the more commonly used homopolar generators. Still more recently, Powell and Jamison³ considered the possibility of using an IRG to power, first, a railgun and, second, a load of constant resistance and inductance. (The constant-impedance load might be used to model, say, a plasma-heating device in an electrothermal gun.) Whereas the latter application did not appear to be particularly promising, the former application was thought to merit further study.

In this report we will be concerned with extending the work of Ref. 3 to investigate in detail the possibility of using an IRG to power a railgun (RG).

¹Marshall, R.A., "A Reusable Inverse Railgun Magnetic Flux Compression Generator to Suit the Earth-to-Space-Rail-Launcher," IEEE Trans. Magn. MAG-20, 223 (1984).

²Benford, J., Kares, R. Brooks, A., and Goldman, E., "High Energy Railgun Designs," IEEE Trans. Magn. MAG-20, 407 (1984).

³Powell, J.D. and Jamison, K.A., "Analysis of an Inverse Railgun Power Source," IEEE Trans. Magn. MAG-22, 1669 (1986).

In particular, we will account more accurately than before for the resistance of both sets of rails and both armatures. A more exact treatment was considered necessary since our previous analysis indicated that the operation of the device in this configuration was highly sensitive to the resistance of both the IRG and the load.

The report is organized as follows. In Sec. II, the model is discussed and the governing equations presented. In Sec. III, an exact analytic solution to these equations is obtained for the case in which resistive effects are neglected. Most of the material in this section is presented in a more abbreviated version in Ref. 3. In Sec. IV, resistance is included in the calculations. Finally, in Sec. V the results are summarized and some indication of future work is given.

II. MODEL AND GOVERNING EQUATIONS

The model to be employed in the calculations is shown schematically in the upper half of Fig. 1. The subscript one is used throughout to denote variables associated with the IRG and the subscript two denotes variables associated with the RG. A seed current of magnitude i_0 flows initially through the two armatures, of mass m_1 and m_2 , and along the rails in the direction indicated. The two armatures are initially located at $x_1 = 0$ and $x_2 = D$, where D is the length of the IRG. At time $t = 0$ an external force is applied to m_1 causing it to move to the right. If the motion is sufficiently rapid the current in the circuit will rise and kinetic energy will be converted into electrical energy. During this time, m_1 is decelerated by the $\vec{J} \times \vec{B}$ force (or magnetic pressure) while m_2 is accelerated. The object is to determine for what parameters the velocity v_2 of m_2 can be maximized.

A more conceptual drawing of the IRG-RG configuration is shown in the lower half of the figure. For reasons indicated in the subsequent analysis, the most desirable design is usually a multi-turn IRG used in conjunction with a single-turn RG. Shown in the drawing is a three-turn IRG. Current is conducted along the rails in the direction indicated by the arrows.

It is convenient in all subsequent analysis to use dimensionless variables for all quantities associated with the operation of the IRG. The manner in which these quantities is made dimensionless is shown in Table I. The method of normalization was rather arbitrary and chosen to make the governing equations as simple as possible. In the table, L_1' is the inductance per unit length of the IRG, σ is the conductivity of the rails, μ is the free-space permeability, and v_n is given by

$$v_n = \left(\frac{2 E_e}{m_1} \right)^{1/2}, \quad (2.1)$$

where E_e is the electrical energy initially in the circuit, i.e., $\frac{1}{2} L_1' i_0^2 D$. Physically, v_n is the velocity reached by the IRG armature if it was started from rest and accelerated to the left by the magnetic force of the seed current, with no energy transferred to the RG armature.

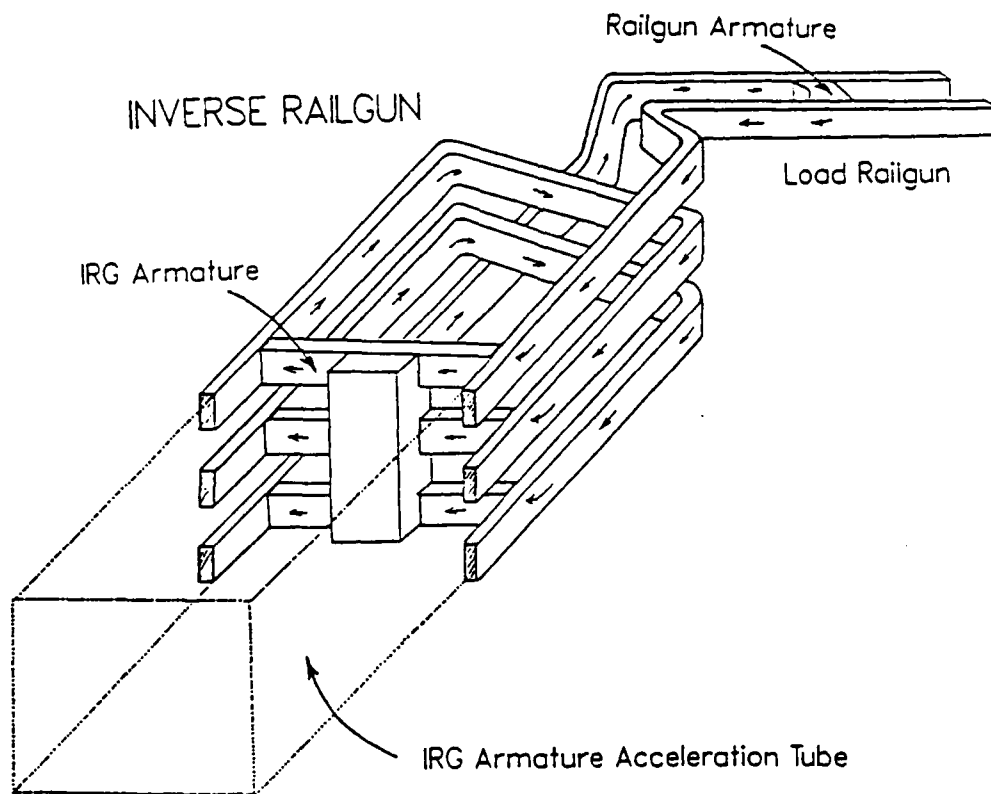
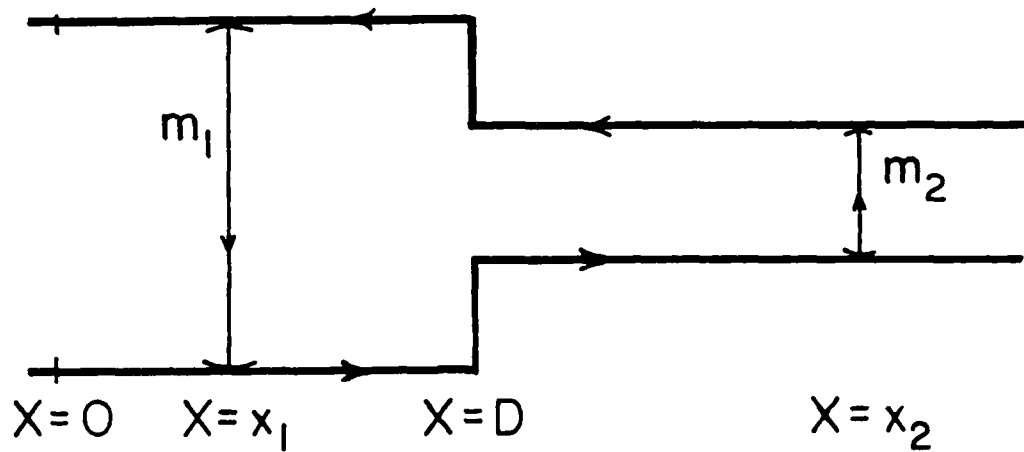


Figure 1. Schematic diagram of model and conceptual drawing of IRG-RG configuration.

TABLE I. Normalization of Variables

<u>Quantity</u>	<u>Symbol</u>	<u>Normalizing Factor</u>	<u>Symbol for Dimensionless Quantity</u>
Current	i	i_0	I
IRG-Armature Position	x_1	D	\bar{x}_1
RG Armature Position	x_2	D	\bar{x}_2
IRG Armature Velocity	v_1	v_n	\bar{v}_1
RG Armature Velocity	v_2	v_n	\bar{v}_2
Resistance	R	$L'_1 v_n$	\bar{R}
Inductance	L	$L'_1 D$	\bar{L}
Time	t	D/v_n	τ
IRG Skin Depth	δ_1	$\left(\frac{D}{\mu\sigma v_n}\right)^{1/2}$	$\bar{\delta}_1$
RG Skin Depth	δ_2	$\left(\frac{D}{\mu\sigma v_n}\right)^{1/2}$	$\bar{\delta}_2$
Distance Beneath Rail Surface	y	$\left(\frac{D}{\mu\sigma v_n}\right)^{1/2}$	\bar{y}

The equations which govern the behavior of the IRG-RG configuration follow directly from the equations of motion of each armature and Kirchoff's law for the circuit. In the dimensionless coordinates just defined these equations become

$$\ddot{\bar{x}}_1 = \dot{\bar{v}}_1 = -I^2/2 \quad , \quad (2.2)$$

$$\ddot{\bar{x}}_2 = \dot{\bar{v}}_2 = \frac{I^2}{2 \alpha \beta} \quad , \quad (2.3)$$

and

$$\frac{\partial}{\partial \tau} (\bar{L} I) + I \bar{R} = 0 \quad . \quad (2.4)$$

The dots denote differentiation with respect to the dimensionless time τ , and \bar{L} and \bar{R} denote the dimensionless inductance and resistance of the complete system (see Table I). It is evident that \bar{L} is given by

$$\bar{L} = 1 - \bar{x}_1 + \frac{1}{\beta} (\bar{x}_2 - 1) \quad , \quad (2.5)$$

while \bar{R} depends upon the specific form of the resistance assumed for the IRG, the RG, and the two armatures. The quantities α and β are given by

$$\alpha = m_2/m_1 \quad (2.6)$$

and

$$\beta = L'_1/L'_2 \quad (2.7)$$

where L'_2 is the inductance per unit length of RG. In the most general case there is a force acting upon the IRG armature, but in cases to be studied here it is assumed for simplicity that the force acts impulsively at $t = 0$, providing m_1 some initial velocity, and is zero afterwards. The force is therefore not included in Eq. (2.2).

Equations (2.2)-(2.4) must be solved subject to the initial conditions

$$\begin{aligned} \bar{x}_1 (\tau = 0) &= 0 \\ \bar{v}_1 (\tau = 0) &= \sqrt{\gamma} \\ \bar{x}_2 (\tau = 0) &= 1 \\ \bar{v}_2 (\tau = 0) &= 0 \\ I (\tau = 0) &= 1 \end{aligned} \quad (2.8)$$

The quantity γ represents the ratio of the initial kinetic energy given to m_1 and the initial electrical energy associated with the seed current. Thus, we have

$$\gamma = m_1 v_{10}^2 / L' i_0^2 D \quad (2.9)$$

where v_{10} is the initial (real) velocity of the IRG armature. As will be seen, the parameters α , β , and γ are very influential in determining the operation of the IRG-RG system.

III. SOLUTION FOR NO RESISTANCE

In the limiting case in which the resistance \bar{R} of the IRG-RG configuration is neglected, an exact analytic solution of Eqs. (2.2)-(2.4) can be obtained. While the solution is not useful for obtaining quantitative results, it does provide some insight for understanding the case in which resistance is included.

To solve Eqs. (2.2)-(2.4) we make the transformation

$$\begin{aligned} X &= \bar{x}_1 + \alpha \beta \bar{x}_2 \\ Y &= \bar{x}_2 - \beta \bar{x}_1 \end{aligned} \quad (3.1)$$

After obtaining a first integral of (2.4), we find

$$\ddot{X} = 0 \quad , \quad (3.2)$$

$$\ddot{Y} = \frac{I^2}{2 \alpha \beta} (1 + \alpha \beta^2) \quad , \quad (3.3)$$

and

$$I = \frac{\beta}{Y - 1 + \beta} \quad . \quad (3.4)$$

The solution to Eq. (3.2) obeying the initial conditions specified in (2.8) is evidently

$$X = \sqrt{\gamma} \tau + \alpha \beta \quad . \quad (3.5)$$

Substituting (3.4) into Eq. (3.3) and integrating we obtain

$$\dot{Y} = \pm \left[\beta^2 \gamma + \left(\frac{1 + \alpha \beta^2}{\alpha} \right) \left(1 - \frac{\beta}{Y - 1 + \beta} \right) \right]^{1/2} \quad . \quad (3.6)$$

The lower sign is to be taken in Eq. (3.6) prior to the time \dot{Y} goes to zero, while the upper sign is to be taken for later times. Finally, integrating (3.6) again yields τ versus Y , i.e.,

$$\begin{aligned} \tau &= \frac{\beta^2 \sqrt{\gamma}}{b} + \frac{\beta(1/\alpha + \beta^2)}{b^{3/2}} \tanh^{-1}(\beta \sqrt{\gamma/b}) \pm \frac{\sqrt{uv}}{b} \\ &+ \frac{\beta(1/\alpha + \beta^2)}{b^{3/2}} \tanh^{-1} \sqrt{\frac{u}{bv}} \end{aligned} \quad (3.7)$$

where

$$b = \beta^2 \gamma + 1/\alpha + \beta^2 , \quad (3.8)$$

$$u = \beta^2 \gamma (\beta - 1) - 1/\alpha - \beta^2 + bY , \quad (3.9)$$

and

$$v = \beta - 1 + Y . \quad (3.10)$$

Once X and Y are known, \bar{x}_1 and \bar{x}_2 follow from the transformation inverse to Eq. (3.1), namely,

$$\bar{x}_1 = \frac{X - \alpha \beta Y}{1 + \alpha \beta^2} \quad (3.11)$$

and

$$\bar{x}_2 = \frac{Y + \beta X}{1 + \alpha \beta^2} . \quad (3.12)$$

It is evident from the foregoing analysis that the operation of the IRG-RG system depends principally upon the parameters α , β , and γ . One is normally interested in employing the device for values of α which are fairly small and values of γ which are fairly large. The first condition is necessary to achieve large velocities of the railgun projectile, and the second condition is necessary to achieve significant current gain in the system.

It is furthermore evident that for a given α and γ the parameter β can be varied so as to optimize the velocity imparted to the projectile m_2 . It is fairly obvious physically, and can be shown mathematically, that the optimum value of β is one which allows the IRG armature to be completely decelerated just at the time it reaches the end of the IRG gun tube, i.e., at $x_1 = D$. At later times its velocity is negative and the armature accelerates slowly to the left. For values of β which are smaller than the optimum value, m_1 will not be completely decelerated and whatever kinetic energy it has at the end of the gun tube, as well as whatever electrical energy is stored in the circuit, cannot be recovered. On the other hand, for values of β larger than optimum, m_1 is decelerated too fast and "bounces back" toward the left with a substantial portion of its kinetic energy. Again, this energy cannot be recovered. In practice, β can be varied by changing the configuration of the bore and/or the number of turns employed by one or both guns. In subsequent analysis, we will hold L_2' fixed and vary L_1' to achieve the desired value.

We have plotted the solution represented by Eqs.(3.11) and (3.12) for various values of α and γ and varied β until the maximum (final) value of \bar{v}_2 , denoted by \bar{v}_{2f} , was obtained. Typical of the results are those shown in Figs. 2-4 in which are plotted the dimensionless variables, \bar{x}_1 , \bar{x}_2 , \bar{v}_1 , \bar{v}_2 , and I versus the dimensionless time τ for three different sets of values of α and γ .

For the case in which $\alpha = 0.1$ and $\gamma = 14.0$ (Fig. 2), the optimum value of β was found to be about 3.8 with both higher and lower values of β producing smaller final velocities of m_2 . As can be seen in the figure the final velocity \bar{v}_{2f} is about 11.7 or about three times the initial value of \bar{v}_1 . This velocity is reached just subsequent to the time m_1 reverses its direction at the end of the IRG gun tube and little change in the velocity occurs thereafter. The final value of \bar{x}_2 shown in the figure is about 4.7 so it is evidently necessary that the railgun be nearly four times longer than the IRG to achieve this final velocity. Final values of \bar{v}_1 and \bar{x}_1 are -0.69 and 0.86, respectively.

Probably the most significant result presented in Fig. 2 is the current profile. The small width of the pulse, as well as the fact that the maximum current is about 9.3 times the initial value, places a rather severe limitation on the operation of the IRG for these values of the parameters. If, for example, we choose $E_e = 25$ kJ, $m_1 = 1$ kg, $D = 1$ m, and $L'_2 = 0.4$ μ H/m, then $v_{2f} \approx 2620$ m/s, $i_0 \approx 180$ kA, and $i_{\max} \approx 1.7$ MA. Such large currents are likely to be deleterious to the rails of any reasonably sized railgun. Furthermore, the half-width of the pulse is only about one-sixth of the total acceleration time (~ 2.7 ms for the real parameters indicated above). Thus, the force on the armature is very nonuniform in time. This situation is known from conventional-gun studies to be very undesirable; not only is damage to the projectile likely to be severe, but the system is also inefficient.

The high maximum current can be considerably reduced provided the IRG armature is made more massive. Such an effect is shown in Fig. 3 in which are plotted results for the same value of γ , 14.0, but with α reduced by a factor of ten. The optimum value of β for this case turns out to be about 12.0. Final velocities and positions are given by $\bar{v}_{2f} = 36.9$, $\bar{x}_{2f} = 13.2$, $\bar{v}_{1f} = -0.69$, and $\bar{x}_{1f} = 0.85$. The maximum dimensionless current reached is again about 9.3 but the real current is less than in the case considered previously. If, for example, we choose $E_e = 25$ kJ, $D = 1$ m, and $L'_2 = 0.4$ μ H/m, as before, but choose $m_1 = 10$ kg in order to reduce α by a factor of ten, we find $v_{2f} \approx 2608$ m/s, $i_0 = 102$ kA, and $i_{\max} = 949$ kA. The final velocity of the projectile is therefore about the same as the previous case but the current peak has been reduced by nearly a factor of two. The half-width of the peak, however, is still small relative to the total acceleration time, about 8.7 ms for these parameters.

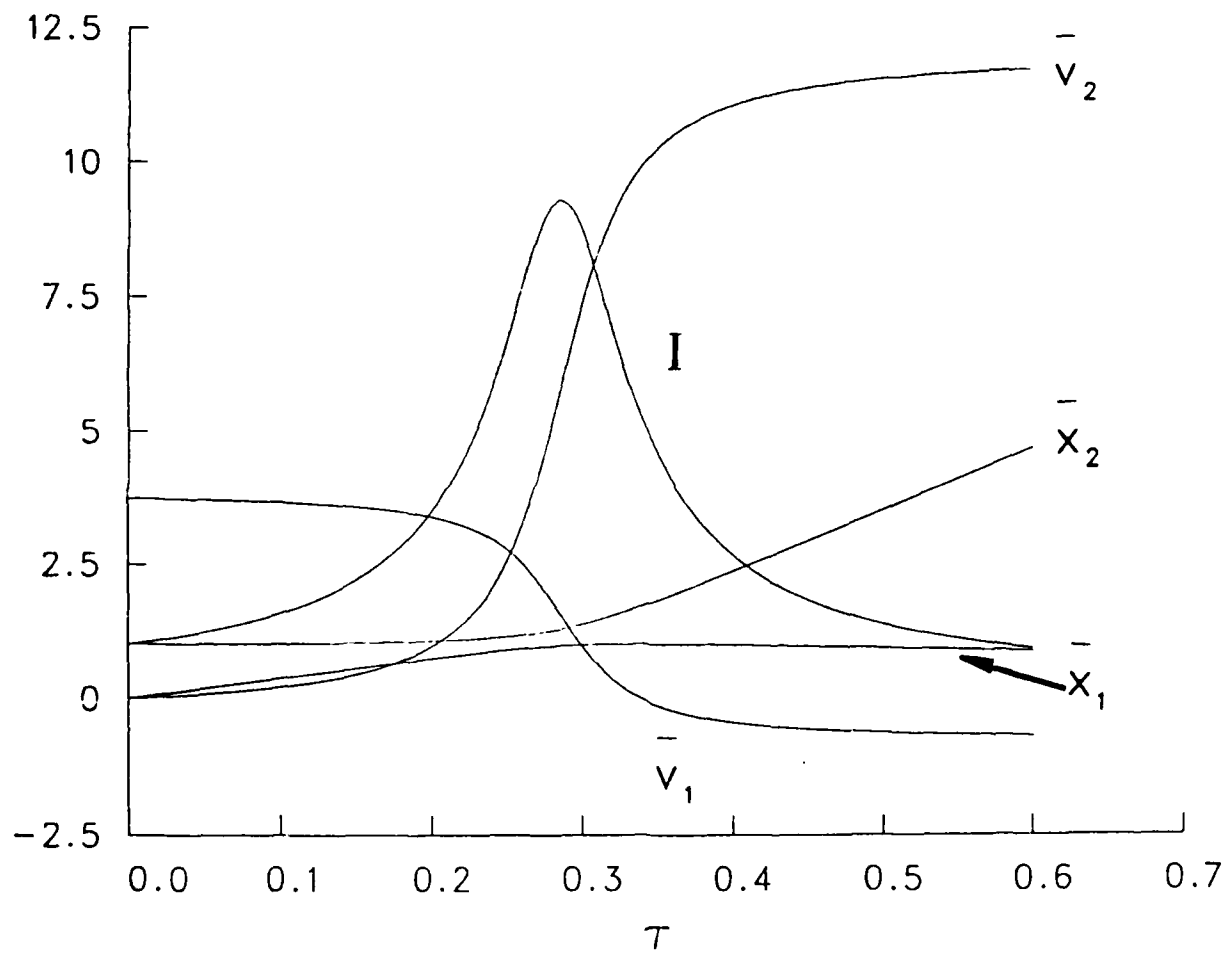


Figure 2. Performance of IRG with no resistance ($\alpha = 0.1, \gamma = 14.0, \beta = 3.8$).

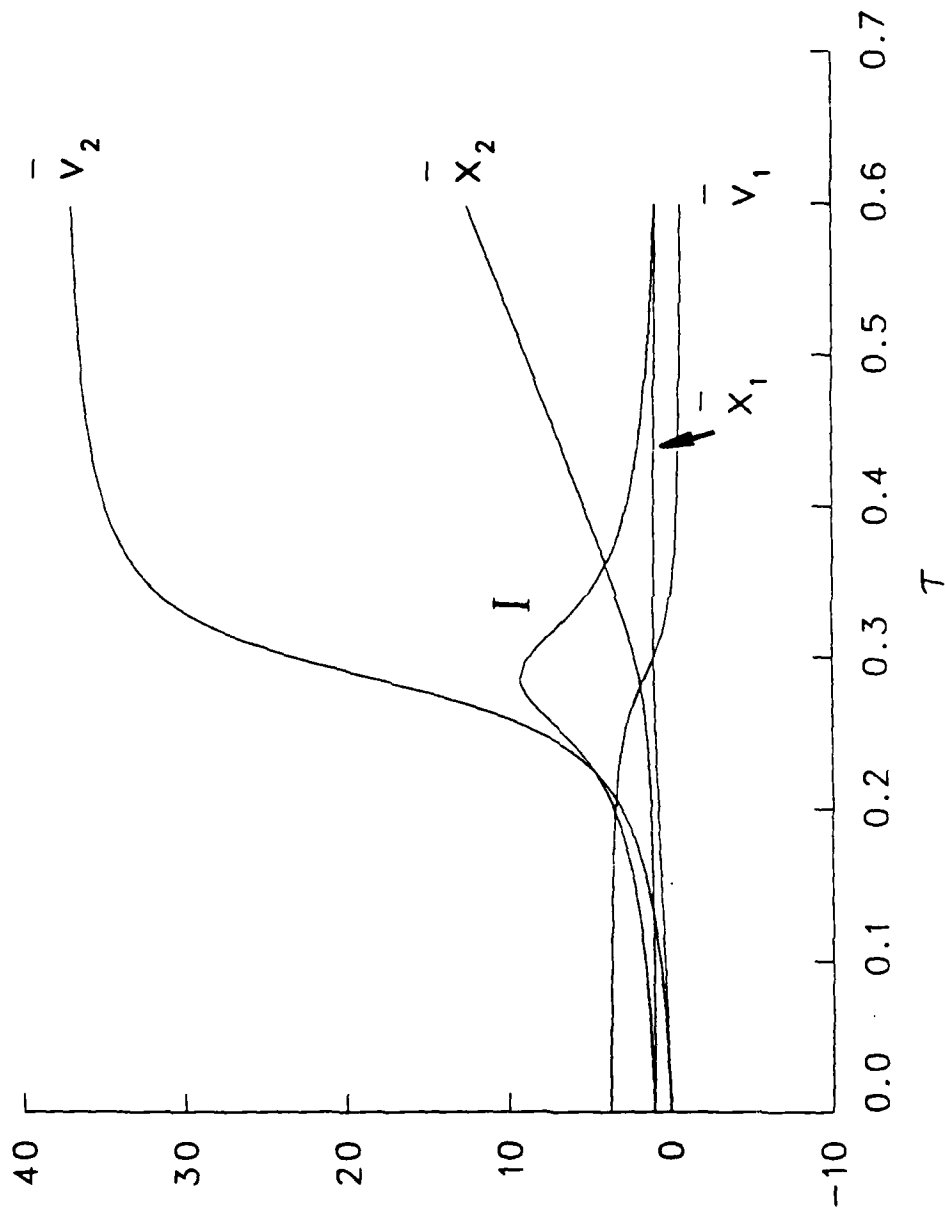


Figure 3. Performance of IRG with no resistance ($\alpha = 0.01$, $\gamma = 14.0$, $\beta = 12.0$).

The results obtained for this case, compared to those of the previous example, can be explained approximately as follows. Here, the more slowly moving projectile will compress the flux entrained in the bore less rapidly than before. Consequently, comparable current gain (i/i_0) and a retarding force sufficient to decelerate the IRG armature can be achieved only if L_2' (or β) is increased. Now, however, the initial current i_0 will be smaller for a fixed stored electrical energy and the maximum real current will be correspondingly smaller. The smaller currents also lead to a less rapid acceleration of the projectile m_2 so that the time required for energy transfer to occur is much longer in the second case. Thus, a rather long RG will be required and the additional length is a disadvantage relative to the previous case. In general, a compromise between very high currents and very long rails must be made. This point is discussed further when resistive effects are considered.

The current maximum can be made still smaller if one is willing to employ smaller values of the energy ratio, γ . It is obvious that then less flux compression should occur and the current gain, i/i_0 , should be smaller than for large values of γ . Results of a calculation for $\alpha = 0.01$, as before, but γ reduced by 50%, i.e., $\gamma = 7.0$, are shown in Fig. 4. Here, the optimum value of β was found to be about 10.8 and final values of the pertinent variables were: $\bar{v}_{2f} = 27.0$, $\bar{x}_{2f} = 17.5$, $\bar{v}_{1f} = -0.27$, and $\bar{x}_{1f} = 0.92$. The maximum relative current, I_{\max} , is now only about 4.8, i.e., about a factor of two smaller than before.

If we assume $m_1 = 10$ kg, $D = 1$ m, $L_2' = 0.4$ $\mu\text{H/m}$, as before, but now take $E_e = 50$ kJ so that γ is half the value considered in the previous example, we find: $\bar{v}_{2f} = 2700$ m/s, $i_0 = 152$ kA, and $i_{\max} = 725$ kA. Thus, the maximum current has been reduced by about 25% from that in the previous case. Again, however, the low currents require exceedingly long RGs to effect the energy transfer. Furthermore, if the value of γ becomes too close to unity, so that the initial electrical energy is comparable to the initial kinetic energy of the armature, the IRG becomes a rather impractical device; the entire acceleration process may as well then be done electrically.

For fixed values of α and γ the IRG must be designed so that the optimum value of β is achieved. It is therefore important to know how sensitive the final velocity \bar{v}_{2f} is to the variation of β . To partially answer this question we have plotted in Fig. 5 the terminal velocity \bar{v}_{2f} as a function of β . The parameters γ and α were held fixed at 14.0 and 0.1, respectively, as for the case studied in Fig. 2. For values of β to the left of the vertical line ($\beta = 3.8$), no reversal of the IRG armature occurs. As pointed out previously the kinetic energy carried by m_1 as well as the stored electrical energy is then lost when m_1 reaches the end of the gun tube and the system is very inefficient. Consequently, the value of \bar{v}_{2f} drops quite remarkably as one proceeds to the left of the vertical line. For values of β to the right of the line, reversal always occurs. As β increases from the optimum value, however,

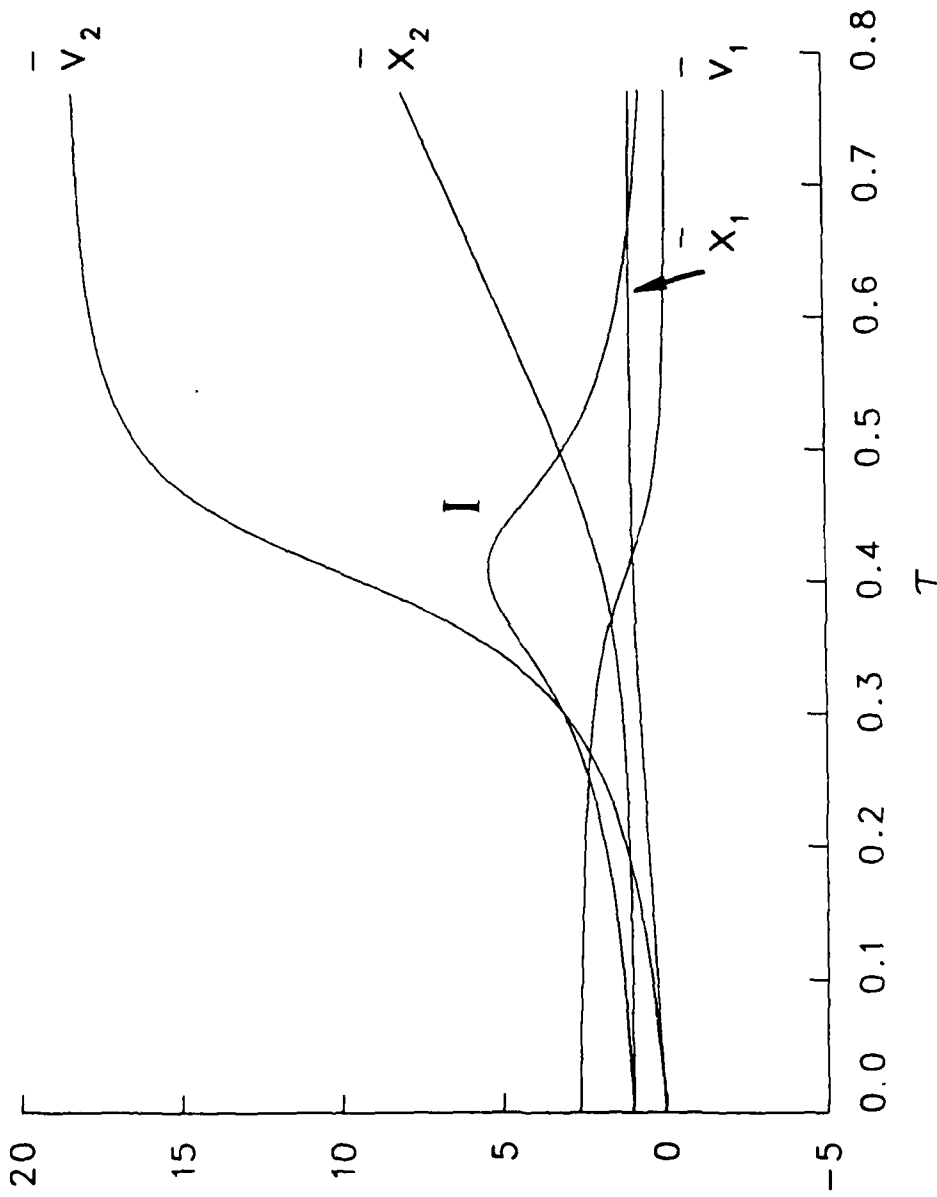


Figure 4. Performance of the IRG with no resistance ($\alpha = 0.01, \gamma = 7.0, \beta = 10.8$).

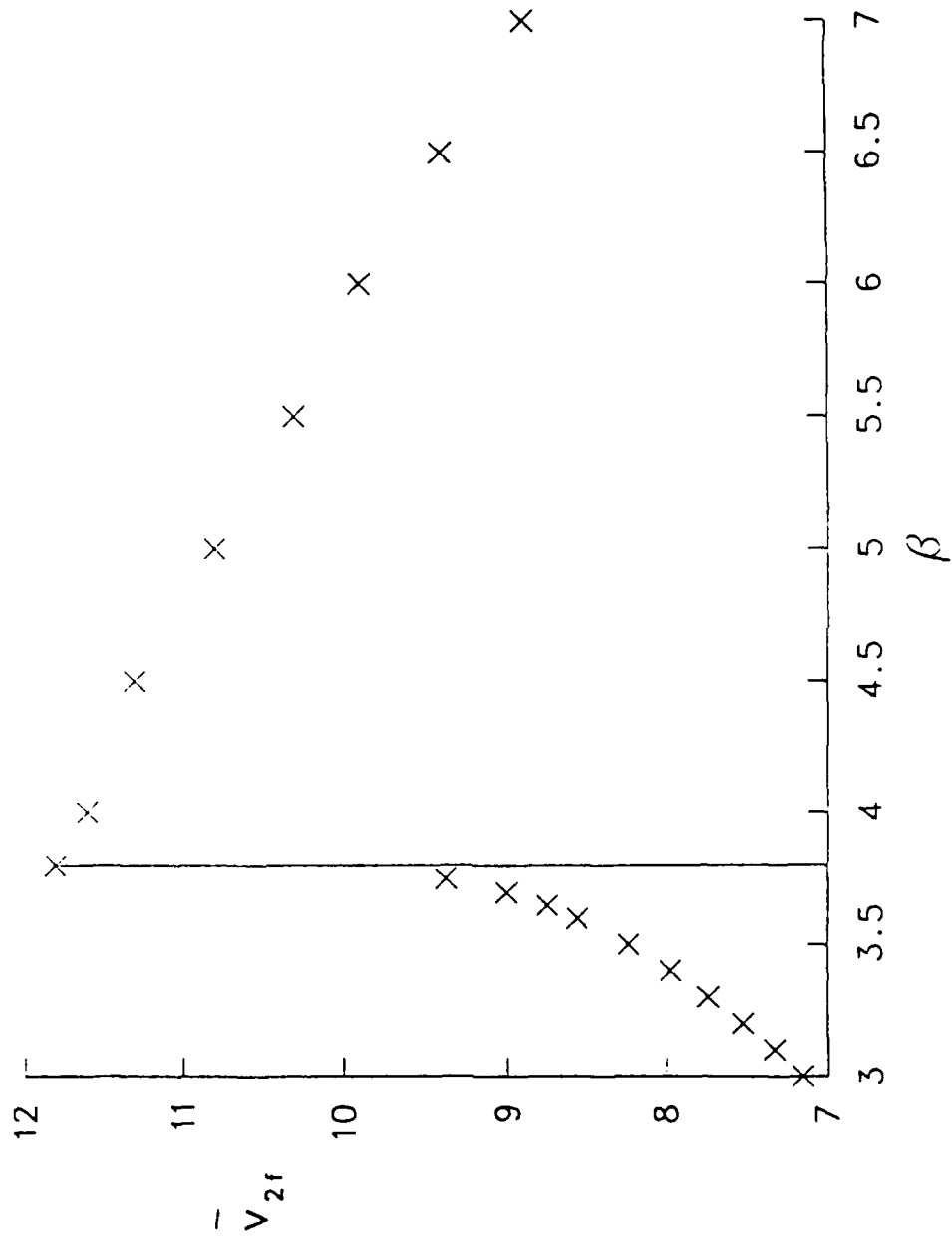


Figure 5. Effect of varying β on maximum velocity achieved by railgun armature.

reversal takes place farther away from the end of the gun tube and m_1 accelerates backwards with a greater portion of its initial kinetic energy. Again efficiency is lost. Obviously, however, it is far better to overestimate slightly, rather than to underestimate, the appropriate value of β . All calculations in Fig. 5 were terminated when $x_1 = 1$ if no reversal occurred, or when \bar{v}_{2f} had approached a terminal value when reversal did occur.

IV. EFFECTS OF RESISTANCE

A. Analysis

When resistance is included in the calculation, the situation can be expected to change substantially. In particular, for a given value of L_1' the current gain should be smaller than for the resistanceless case and consequently the retarding force on m_1 is smaller. It will therefore be necessary to increase the inductance ratio β in order to decelerate m_1 to zero velocity just at the end of the IRG gun tube. However, the same basic conclusions that held for the resistanceless case should hold here as well.

We consider now the effects of resistance on the performance of the IRG configuration. The resistance of both sets of rails is considered as well as that of both armatures. It is assumed that, prior to time $t = 0$, the current in the IRG is brought up to its initial value of i_0 by, say, discharging a capacitor in a time t_0 . The current during this initial discharge time is assumed to vary sinusoidally so that we have

$$i = i_0 \sin \left[\frac{\pi (t + t_0)}{2 t_0} \right], \quad -t_0 \leq t \leq 0 \quad (4.1)$$

and m_1 and m_2 are assumed to remain fixed at $x_1 = 0$ and $x_2 = D$, respectively. The assumption should be quite reasonable since typically t_0 is small compared to the total time of acceleration.

Now during the discharge time and subsequently after the armature is moving, the resistance of the IRG rails is determined by the IRG skin depth, or the extent to which the current has penetrated beneath the rail surface. It is furthermore evident that while m_1 is moving forward, the skin depth is independent of position along the rail surface and the total resistance is given by

$$R_1 = \frac{2N^2 (D - x_1)}{oh_1 \delta_1} \quad (4.2)$$

In Eq. (4.2), N represents the total number of turns in the IRG (see Fig. 1), δ_1 is the skin depth, and h_1 is the total height. Thus, each turn has height h_1/N and the turns are series-connected. Equation (4.2) does not hold, of course, once the armature reverses its direction and the skin depth now depends upon position along the rails. In the numerical calculations, however, the

resistance of the IRG during this time will be neglected since it is generally small relative to that of the RG.

It is shown in the appendix that the skin depth inside any of the conductors (IRG rails, RG rails, or armature) that constitute the bore of the IRG-RG system is given at any time by

$$\delta = - \frac{B_S}{[\hat{n} \cdot \nabla B]_S} \quad (4.3)$$

Here \hat{n} denotes a unit vector normal to the surface (pointing into the conductor), B is the magnetic induction field, and the subscript S means that the quantity in question is to be evaluated at the conductor surface. For, say, the upper rail in the IRG, $\hat{n} = \hat{a}_y$ and the induction field for $y > 0$ is obtained by solving the standard diffusion equation

$$\frac{\partial B}{\partial t} = \frac{1}{\mu\sigma} \frac{\partial^2 B}{\partial y^2} \quad (4.4)$$

Diffusion in directions other than normal to the conductor surface is neglected. The boundary condition on the field at the surface, needed to solve the equation, is taken to be

$$B_S = B(y=0) = \mu j_1 \quad (4.5)$$

where j_1 is the current per unit height on the rail surface. In assuming the above results we have neglected any dependence of the induction field within the bore of the gun on z and taken the field to have single component $\vec{B} = B\hat{a}_z$. Such an assumption is not expected to affect greatly the skin-depth calculation. If we now write Eqs. (4.2)-(4.4) in terms of the dimensionless variables defined in Table I, we find

$$\delta_1 = - \frac{B_S}{\frac{\partial B_S}{\partial y}} \quad (4.6)$$

$$\frac{\partial B}{\partial \tau} = \frac{\partial^2 B}{\partial y^2} \quad (4.7)$$

and

$$\bar{R}_1 = \frac{CN^2 h_2 (1 - \bar{x}_1)}{h_1 \beta \bar{\delta}_1} \quad (4.8)$$

In Eq. (4.8), C is given by

$$C = \frac{2}{L_2' h_2} \left(\frac{\mu D}{\sigma v_n} \right)^{\frac{1}{2}} \quad (4.9)$$

where h_2 is the railgun height. The IRG inductance gradient has been written as $\beta L_2'$ since we customarily vary β by changing L_1' and hold L_2' as well as the initial electric and kinetic energies fixed.

We next determine how the inductance gradient L_1' of the IRG can be expected to vary as one varies the number of turns and changes the ratio

$$s_1 = h_1/W_1 \quad (4.10)$$

where W_1 represents the rail separation in the IRG. As W_1 and h_1 are varied it is assumed that the cross-sectional area A_1 of the IRG remains fixed. For a rectangular cross-section, single-turn gun the inductance gradient can be approximated by Batteh's formula⁴

$$L_1' = \frac{2\mu}{\pi s_1^2} G(s_1) \quad (4.11)$$

where $G(s_1)$ is given by

$$G(s_1) = s_1 \tan^{-1}(s_1) + \frac{s_1^2}{4} \log(1 + 1/s_1^2) - \frac{1}{4} \log(1 + s_1^2). \quad (4.12)$$

For an N -turn gun of the same geometry, it is expected that the inductance L' would become multiplied by approximately N^2 in keeping with standard results for square-bore guns. If it is finally assumed that the RG is a single-turn square-bore gun, then we obtain from Eq. (4.11) and the arguments above

$$\beta = \frac{L_1'}{L_2'} = \frac{4N^2 G(s_1)}{\pi s_1^2}, \quad (4.13)$$

where we have noted that $G(1) = \pi/4$. Evidently, then, β can be varied by varying the turns N in the IRG as well as by changing the height-to-separation ratio s_1 , until the optimum value is found.

The skin depth of the RG can be determined via considerations analogous to those for the IRG. Here it must be remembered, however, that the current has not been flowing the same length of time at all points along the RG tube. In particular, the current is initiated at any point only when the projectile m_2 arrives at the point in question. Consequently, the RG skin depth δ_2 is a function of x , the position along the gun tube, and the total RG resistance must be found by integrating each contribution along the gun-tube surface. In terms of the usual dimensionless variables we have

⁴Batteh, Jad H., "Momentum Equation for Arc-Driven Railguns," J. Appl. Phys. 56, 3182 (1984). See also, "Arc-Dynamic Calculations in the Railgun," Ballistic Research Laboratory Contract Report No. ARBRL-CR-00521, November 1983.

$$\bar{R}_2 = \frac{C}{\beta} \int_1^{\bar{x}_2} \frac{d\bar{x}}{\delta_2(\bar{x}, \tau)} \quad (4.14)$$

The skin depth $\bar{\delta}_2(\bar{x}, \tau)$ is obtained by solving (4.7) at various points \bar{x} along the RG gun tube and using Eq. (4.6) with subscript one replaced by two.

A problem appears to arise in Eq. (4.14) as $\bar{x} \rightarrow \bar{x}_2$ since $\delta_2 \rightarrow 0$. It is possible to argue, however, that the integral in (4.14) still converges. In fact, in the vicinity of \bar{x}_2 the skin depth is well approximated by the expression valid for constant current, namely,

$$\bar{\delta}_2 = (\pi \Delta \tau)^{1/2} \quad (4.15)$$

where $\Delta \tau$ represents the time the current has been flowing at the point in question. If this expression is substituted into (4.14) and the resulting integral performed, it is possible to show that the contribution to the rail resistance between some point \bar{x}_m (near \bar{x}_2) and \bar{x}_2 is given approximately by

$$\bar{R}'_2 = \frac{2C}{\beta} \left[\frac{v_2 (\bar{x}_2 - \bar{x}_m)}{\pi} \right]^{1/2} \quad (4.16)$$

We finally consider the resistance from each of the armatures m_1 and m_2 . Here it is assumed for simplicity that each armature has the same conductivity as the rails. It is apparent then that the current diffuses into each of the armatures at the same rate as in the IRG rails. We can therefore write

$$\bar{R}_A = \frac{h_2 C}{2 \beta D \bar{\delta}_1} (1 + 1/s_1) \quad (4.17)$$

This result accounts for the resistance of both armatures, but neglects resistive effects associated with the rail-armature interfaces.

The equations above are sufficient to yield the resistances \bar{R}_1 , \bar{R}_2 , and \bar{R}_A as a function of time, and the total resistance \bar{R} in Eq. (2.4) is simply the sum of the three. Our procedure has been to assume a value for β and solve numerically the resulting equations for \bar{x}_1 , \bar{x}_2 , v_1 , v_2 , and I using the assumed value. The parameter β was then varied and the process repeated until the maximum value of v_2 was reached.

B. Numerical Technique

In the numerical solution of the foregoing equations, a simple Euler method was employed for the ordinary differential equations (2.2)-(2.4), and a completely explicit technique for Eq. (4.7). The time step $d\tau$ and grid spacing dy were chosen always to satisfy the stability criterion⁵

$$\lambda = \frac{d\tau}{(dy)^2} \leq 1/2 \quad . \quad (4.18)$$

Typical values used were $d\tau = 0.0005$ and $dy = 0.05$.

A dimensionless length of the entire system, denoted by $\bar{x}_{2\max}$, was then assumed and the system divided into 200 segments so that $d\bar{x}$ in Eq. (4.14) was given by $\bar{x}_{\max}/200$. If subsequent calculations revealed that $\bar{x}_{2\max}$ was too small for m_2 to reach a terminal velocity, or if it was significantly too large, the value was changed appropriately. The diffusion equation, Eq. (4.7), was then solved at every grid point along the x direction in the RG provided that $\bar{x} \leq \bar{x}_2$ in order to determine $\bar{\delta}_2(\bar{x}, \tau)$. We normally found that one hundred grid points of separation dy interior to the rail surface were sufficient to prevent the field from diffusing all the way through the rails during the entire calculation time. It is therefore necessary and assumed that the rail thickness is sufficiently great to prevent complete penetration at any point. A similar calculation was carried out to determine $\bar{\delta}_1$ for the IRG, but only a single point along the x direction was employed since $\bar{\delta}_1$ is independent of x_1 .

Once the skin depths $\bar{\delta}_1$ and $\bar{\delta}_2$ have been calculated, the rail resistances \bar{R}_1 and \bar{R}_2 follow from Eqs. (4.8) and (4.14). The integral in (4.14) was evaluated by using the trapezoidal rule for all grid points between the first and the one just prior to \bar{x}_2 . Between the last grid point and \bar{x}_2 , the contribution to the resistance was approximated via (4.16). Finally the armature resistance was found by use of Eq. (4.17).

The above procedure of solving the diffusion equation in the rails and thereby calculating $\bar{\delta}_1$ and $\bar{\delta}_2$ was carried out at every time step. The resulting resistance was then substituted into Eq. (2.4) and the solution marched forward. The calculation was terminated when x_1 became equal to unity (no direction reversal), or when \bar{v}_2 had clearly approached some asymptotic value (after reversal had occurred). The parameter β was then varied, as discussed before, and the calculation repeated until the optimum value of β was found.

⁵Carnahan, B., Luther, H.A., and Wilkes, J.D., Applied Numerical Methods (Wiley, New York, 1969), Chap. 7.

C. Results

We now consider the results of some calculations undertaken using the above procedure. For each case parameters needed to be specified in the calculation, as well as some of the more significant results, are indicated in Table II.

TABLE II. Values of Parameters in Numerical Calculations

<u>Quantity</u>	<u>INPUT PARAMETERS</u>		
	<u>Fig 6</u>	<u>Fig. 8</u>	<u>Fig. 9</u>
α	0.1	0.01	0.005
γ	14.0	7.0	7.0
N	3	4	5
τ_0 [see Eq. (4.1)]	0.05	0.05	0.05
h_2	2.0 cm	2.0 cm	2.0 cm
A_1	50 cm ²	320 cm ²	320 cm ²
C	2.46	1.84	2.19
D	1 m	0.25 m	0.25 m
	<u>RESULTS</u>		
s_1	1.79	1.09	1.20
h_1	9.5 cm	19 cm	20 cm
β	6.3	15.2	22.5
\bar{v}_{2f}	7.7	18.3	24.6
\bar{x}_{2f}	2.8	8.0	10.0
I_{\max}	16.6	5.40	5.52

Shown in Fig. 6 are results for $\alpha = 0.1$ and $\gamma = 14.0$. (The resistanceless case for these parameters was indicated in Fig. 2.) The cross-sectional area A_1 of the IRG was somewhat arbitrarily chosen to be 50 cm² and a three-turn IRG was found to produce the optimum value of β for the most nearly square bore ($s_1 = 1.79$). The optimum value of the inductance ratio was found to be about 6.3, nearly a factor of two larger than in the resistanceless case. As indicated previously, the higher IRG inductance is necessary to decelerate m_1 when resistive losses cause the current to drop.

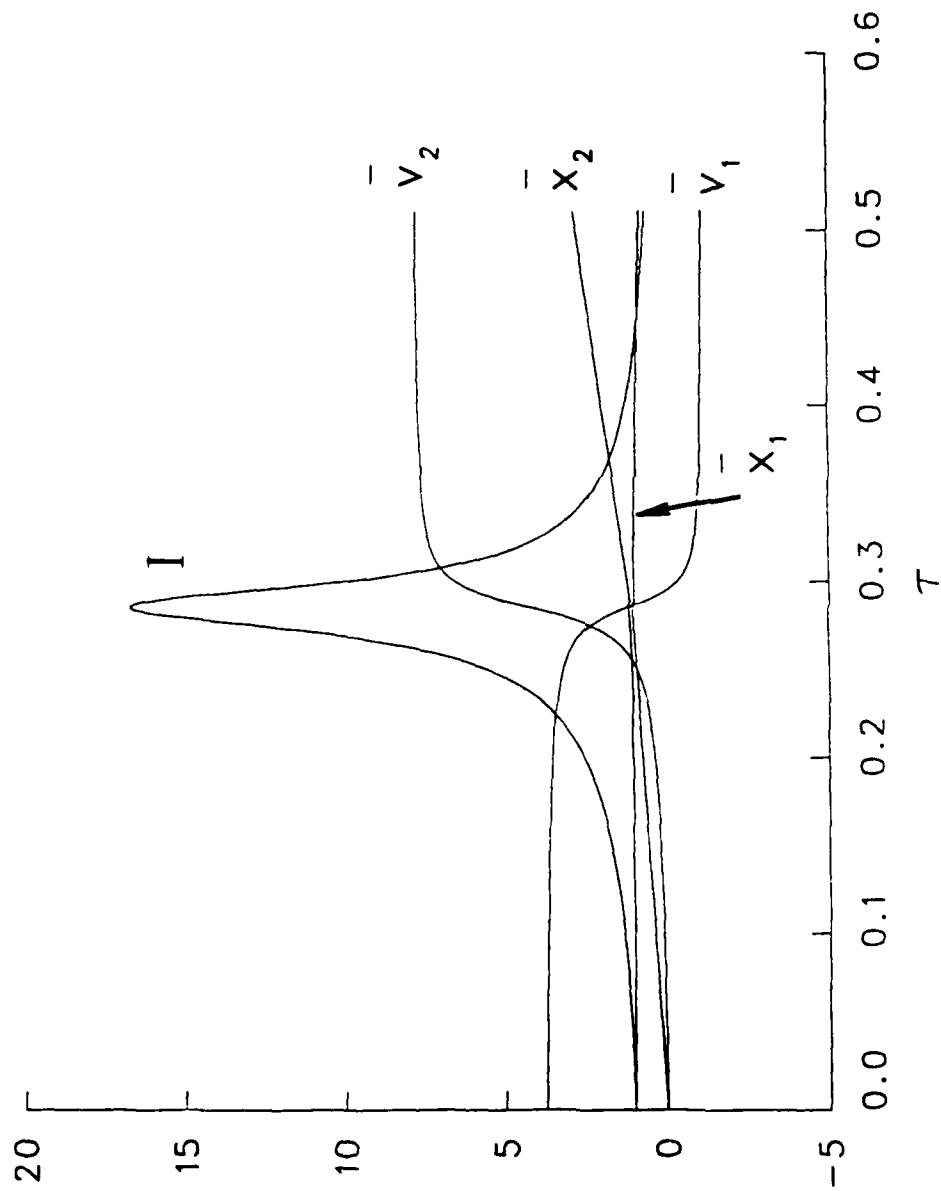


Figure 6. Performance of IRG with resistance ($\alpha = 0.1, \gamma = 14.0, \beta = 6.3$).

It is of some interest to consider the results of Fig. 6 for the same real parameters as indicated for Fig. 2: $E_e = 25$ kJ, $m_1 = 1$ kg, $D = 1$ m, and $L_2' = 0.4$ μ H/m. We then obtain $v_{2f} \approx 1730$ m/s, $i_0 = 140$ kA, and $i_{\max} \approx 2.3$ MA. There is therefore a reduction in projectile velocity by about 35% and an increase in the maximum current by about 35%. The decrease in velocity can be ascribed to the loss in efficiency because of resistive dissipation, and the higher current to the larger inductance gradient L_1' . The length of RG needed, however, is only about 1.8 m (see the entry \bar{x}_{2f} in Table II) as opposed to 3.7 m in the perfect-conductor case. It is rather unlikely that 2.0 cm-high rails could withstand these extremely high currents.

It is next of interest to examine how the potential per unit length along the IRG rails varies as a function of time. We have therefore plotted in Fig. 7 the quantity

$$\bar{V}_1 = \frac{I \bar{R}_1}{2(1 - \bar{x}_1)} \quad (4.19)$$

versus τ for the calculation shown in Fig. 6. At early times, when the total current is nearly constant, the skin depth increases roughly as $\sqrt{\tau}$ and the potential per unit length decreases slightly. Alternatively, one could say that the fairly large current induced at the rail surface when the induction field is first turned on, decreases as the field penetrates the conductor and reduces the field gradient at the boundary. As flux compression occurs, however, and the total current rises, J at the surface must also increase as a consequence of Lenz's law and in an effort to exclude the field from the conductor. The potential therefore rises sharply. Similarly, once the maximum value of I is reached and $\frac{dI}{d\tau}$ becomes negative, a current density in the reverse direction is induced at the surface, again as a consequence of Lenz's law.

This current density is imposed on what was originally there but, if $\frac{dI}{d\tau}$ is sufficiently large in magnitude, the current density at the surface can be oppositely directed from that which initially existed. It is for this reason that the potential becomes negative in Fig. 7 for negative $\frac{dI}{d\tau}$. Evidently, then, the skin depth $\bar{\delta}_1$ is also negative as is the IRG resistance R_1 . The unusual negative resistance results from the uncommon use of a circuit equation, with a constant inductance gradient [see Eq. (2.4)], to describe a situation in which current penetrates beneath the surface of a conductor. In reality, the negative resistance accounts for the decrease in flux beneath the rail surface as the current drops.

It is evident from the results of Fig. 6 and the discussion in Sec. III that the magnitude of the current pulse needs to be reduced, and that such an effect can be accomplished by increasing the IRG armature mass m_1 as well as decreasing the energy ratio γ . It is furthermore obvious that decreasing the resistance will lead to greater efficiency of the IRG. The resistance can be decreased primarily by increasing the bore size, A_1 , and decreasing the length, D . Results of a calculation in which these changes have been effected

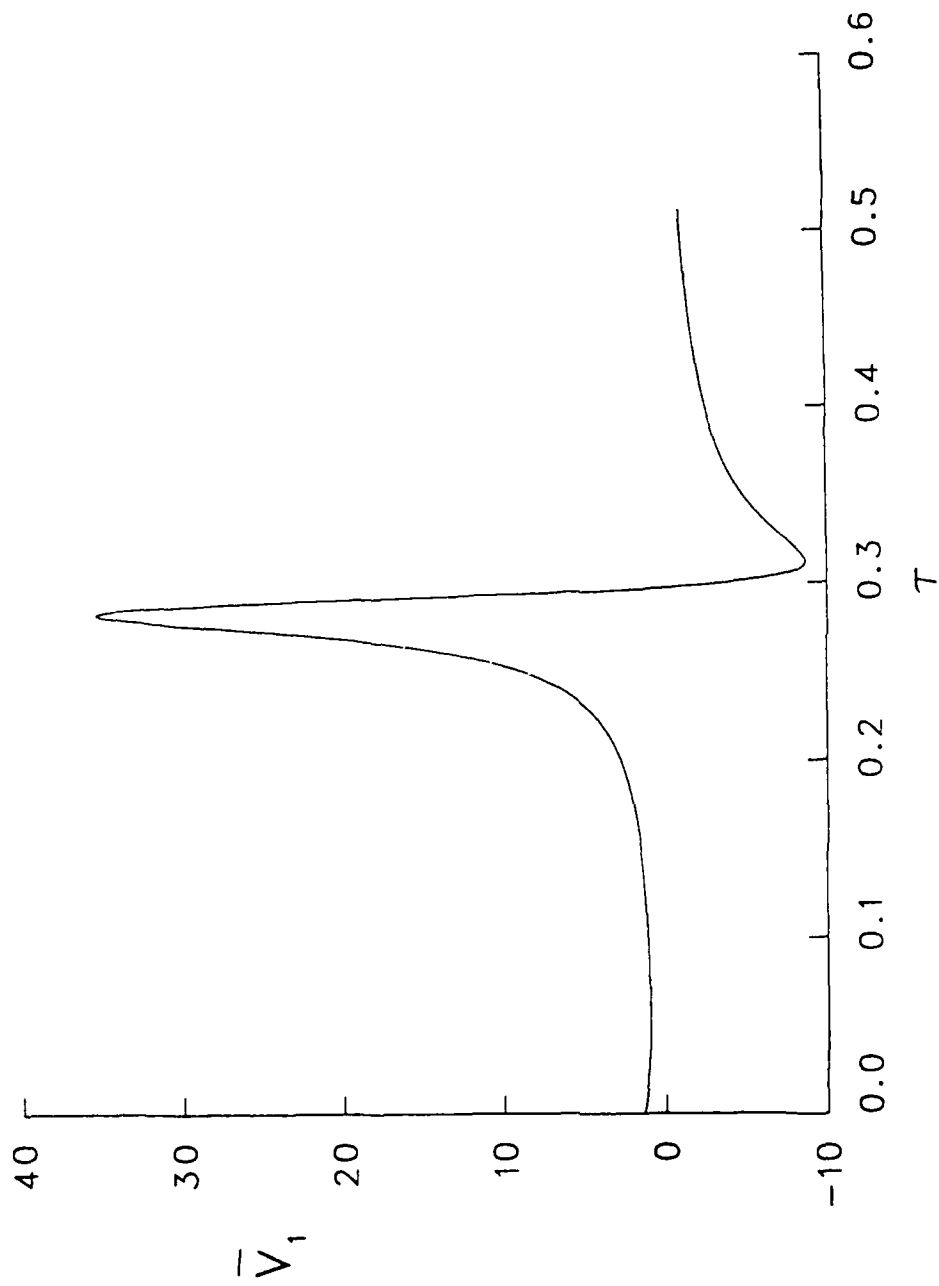


Figure 7. Potential per unit length along IRG rails.

are shown in Fig. 8 with pertinent input parameters as well as some of the more significant results in Table II. Specifically, D was reduced to 0.25 m and A_1 increased to 320 cm². Values of α and γ were the same as for the resistanceless calculation in Fig. 4, i.e., 0.01 and 7.0, respectively. The four-turn IRG was found to give the closest approximation to a square bore ($s_1 = 1.09$) and an inductance-gradient ratio of 15.2 was necessary to decelerate m_1 .

If we choose as real parameters $m_1 = 10$ kg, $D = 0.25$ m, $E_e = 50$ kJ, and $L'_2 = 0.4$ μ H/m (the same as for Fig. 4 except that D has been reduced as discussed), then $v_{2f} \approx 1830$ m/s, $i_0 \approx 257$ kA, and $i_{\max} \approx 1.4$ MA. The reduction in velocity (about 30%) from that obtained in Fig. 4 results from a decrease in efficiency because of resistive losses. The higher currents result from the greater flux compression associated with the larger inductance ratio β , as well as the higher initial current caused by the smaller value of D . The length of the RG needed to achieve this final velocity is about seven times the length of the IRG (see Table II). For $D = 0.25$ m, this length is 1.75 m, a reasonable value.

If α is made still smaller, say, 0.005, smaller peak currents can again be achieved at the expense of longer rails. In Fig. 9 are results of a calculation for $\gamma = 7.0$, as before, but $\alpha = 0.005$. Additional input parameters are the same as in the previous example, except that a five-turn IRG was found to produce the best approximation to a square bore ($s_1 = 1.20$). The optimum value of β was found to be $\beta = 22.5$. If we take for real parameters $D = 0.25$ m, $E_e = 50$ kJ, and $L'_2 = 0.4$ μ H/m, as in the previous example, but increase m_1 to 20 kg, then we find $v_{2f} \approx 1740$ m/s, $i_0 \approx 210$ kA, and $i_{\max} \approx 1.2$ MA. The RG length needed to achieve this velocity is about 9D, i.e., about 2.25 m for $D = 0.25$ m. The reduction in velocity by about 5% from that obtained previously can be attributed to the higher resistance of the five-turn gun.

IV. SUMMARY AND CONCLUSIONS

It appears that satisfactory coupling of energy between the IRG and RG is theoretically possible. Other types of load,³ in a similar switchless configuration, that we have investigated have not proved nearly so satisfactory. The principal reason that the IRG-RG combination works reasonably well is apparently the time variation of the RG impedance. In particular, both the resistance and inductance are very low at early times when flux compression is necessary to achieve current gain.

The major disadvantage of using the IRG to power a railgun appears to be the high peak-to-average current. This problem can be ameliorated to some extent by judicious choice of the initial electrical energy in the IRG and a careful choice of the IRG armature mass. Specifically, small values of both α (ratio of RG projectile mass and IRG armature mass) and γ (ratio of initial kinetic and electrical energies associated with the IRG) produce smaller-height, larger-width current pulses.

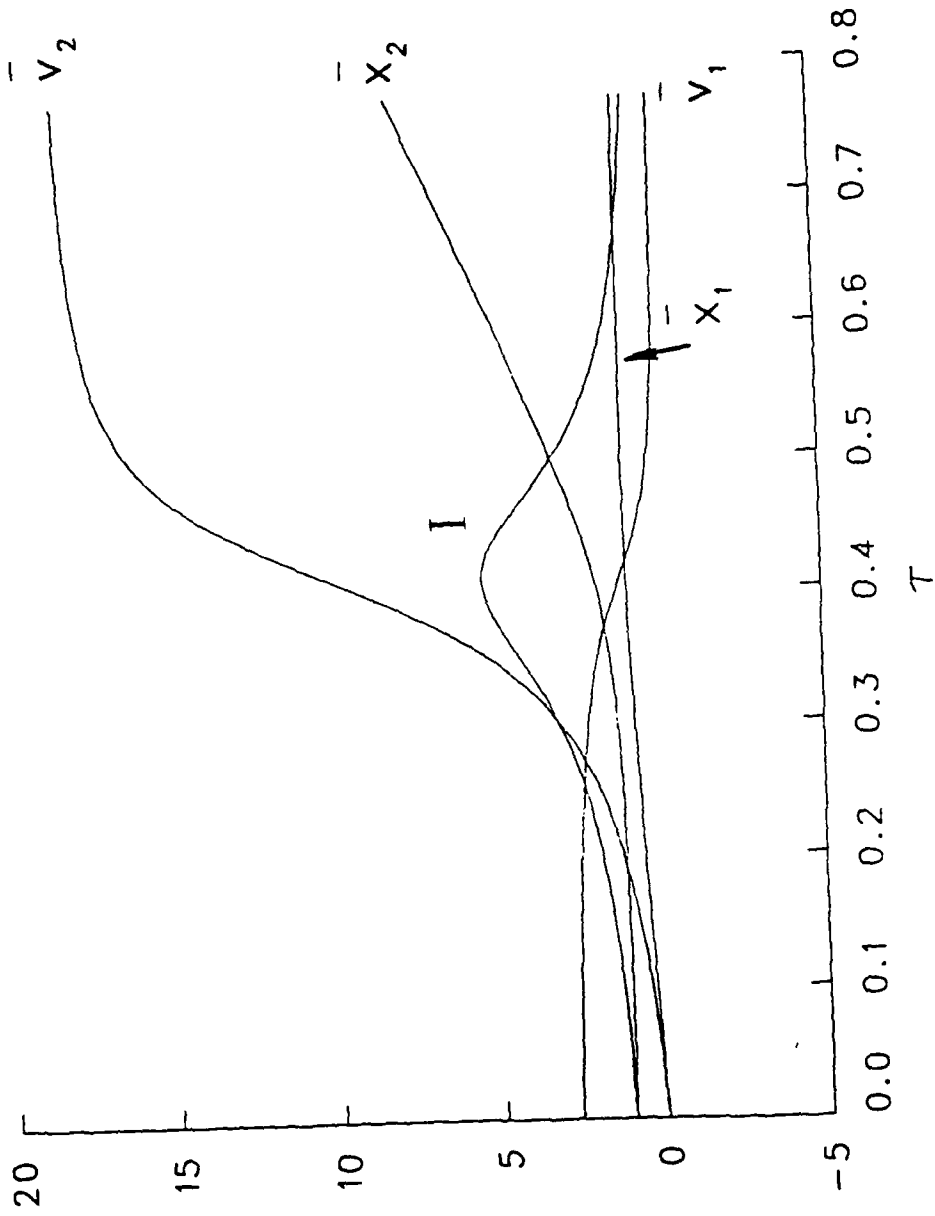


Figure 8. Performance of the IRG with resistance ($\alpha = 0.01$, $\gamma = 7.0$, $\beta = 15.2$).

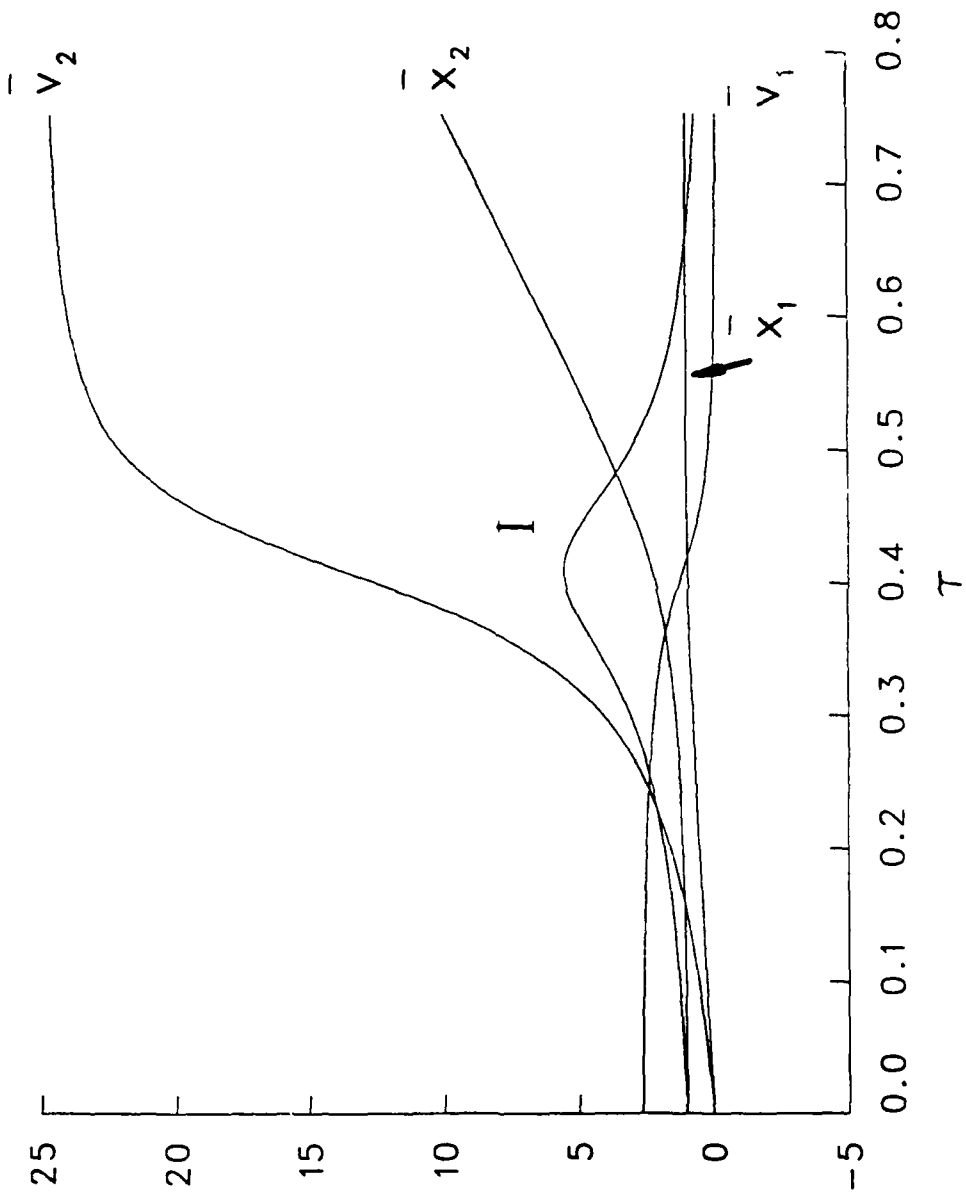


Figure 9. Performance of IRG with resistance ($\alpha = 0.005, \gamma = 7.0, \beta = 22.5$).

Other possibilities, not investigated, also exist for flattening the current profile: For example, Marshall⁵ has considered a configuration in which the IRG inductance gradient is not constant, but rather is larger at the breech than muzzle. A cursory examination indicates that this design would cause the current to rise faster and hence be more nearly constant. The effect can be achieved by varying the number of turns on the IRG as one proceeds from breech to muzzle. It is also possible that use of nonimpulsive driving forces could produce more nearly constant current, but we have not thus far been able to find any reasonable force profile for obtaining the desired effect.

In addition to problems associated with the current profile, other areas appropriate for future investigation include accounting for additional losses and considering designs which allow for switching. Among the losses not accounted for here, for example, is the stray inductance between the IRG and RG. This loss was not included in our analysis since no reliable estimate of its value was known. A number of possibilities for enhancing energy coupling between the IRG and RG (and other types of load) exist if switching is permitted. It would, for instance, be of interest to examine the effect of switching the load into the circuit only after maximum flux compression has been achieved. We have not previously considered designs which allow for switching because the switching itself constitutes a major practical problem.

REFERENCES

1. Marshall, R.A., "A Reusable Inverse Railgun Magnetic Flux Compression Generator to Suit the Earth-to-Space-Rail-Launcher," IEEE Trans. Magn. MAG-20, 223 (1984).
2. Benford, J., Kares, R., Brooks, A., and Goldman, E., "High Energy Railgun Designs," IEEE Trnas. Magn. MAG-20, 407 (1984).
3. Powell, J.D., and Jamison, K.A., "Analysis of an Inverse Railgun Power Source," IEEE Trans. Magn. MAG-22, 1669 (1986).
4. Batteh, Jad H., "Momentum Equation for Arc-Driven Railguns," J. Appl. Phys. 56, 3182 (1984). See also, "Arc-Dynamic Calculations in the Railgun," Ballistic Research Laboratory Contract Report No. ARBRL-CR-00521, November 1983.
5. Carnahan, B., Luther, H.A., and Wilkes, J.D., Applied Numerical Methods (Wiley, New York, 1969), Chap. 7.
6. Powell, J.D., "Thermal-Energy Transfer from Arc to Rails in an Arc-Driven Railgun," IEEE Trans. Magn. MAG-20, 395 (1984). See also Ballistic Research Report No. ARBRL-TR-02530, October 1983.

LIST OF MOST COMMONLY USED SYMBOLS

NOTATION: IRG = Inverse Railgun; RG = Railgun

Symbol	Quantity
A_1	IRG cross sectional area
B	Magnetic induction field
D	Length of IRG
h_1	Rail height (total) of IRG
h_2	Rail height of RG
i	Current
i_0	Initial current in IRG
I	Dimensionless* current
L/\bar{L}	Real/dimensionless inductance
L'_1	IRG inductance gradient
L'_2	RG inductance gradient
m_1	IRG armature mass
m_2	RG armature mass
N	Number of turns for IRG
R/\bar{R}	Real/dimensionless total resistance
R_1/\bar{R}_1	Real/dimensionless IRG rail resistance
R_2/\bar{R}_2	Real/dimensionless RG rail resistance
R_A/\bar{R}_A	Real/dimensionless resistance of IRG and RG armatures
s_1	Ratio of IRG rail height and rail separation
s_2	Ratio of RG rail height and rail separation
t	Time
v_1/\bar{v}_1	Real/dimensionless IRG armature velocity
v_2/\bar{v}_2	Real/dimensionless RG armature velocity

*For normalization procedure, see Table I.

Symbol	Quantity
v_N	Normalization velocity [see Eq. (2.1)]
V_1/v_1	Real/dimensionless IRG potential per unit length of rail
w_1	IRG rail separation
w_2	RG rail separation
x_1/\bar{x}_1	Real/dimensionless IRG armature position
x_2/\bar{x}_2	Real/dimensionless RG armature position
y/\bar{y}	Real/dimensionless distance beneath rail surface
α	Ratio of RG and IRG armature masses
β	Ratio of IRG and RG inductance gradients
$\delta_1/\bar{\delta}_1$	Real/dimensionless IRG skin depth
$\delta_2/\bar{\delta}_2$	Real/dimensionless RG skin depth
γ	Ratio of initial kinetic and initial electrical energies in IRG
σ	Conductivity
τ	Dimensionless time

APPENDIX

The purpose of this appendix is to derive Eq. (2.4) and to infer from the result a general formula for the skin depth δ .

Consider Fig. 1 and assume as discussed previously that the magnetic induction field in the bore of either gun is given by

$$B_{1,2} = \mu j_{1,2} \quad (\text{A.1})$$

where j represents the total current per unit height. From Maxwell's equations one also has

$$\vec{\nabla} \times \vec{E} = - \frac{\partial \vec{B}}{\partial t} \quad (\text{A.2})$$

where \vec{E} is the electric-field intensity. If Stokes' theorem is applied to (A.2) we find

$$\int \vec{E} \cdot d\vec{\ell} = - \int_S \frac{\partial \vec{B}}{\partial t} \cdot d\vec{A}. \quad (\text{A.3})$$

The integral on the left is the line integral over some closed contour, and that on the right is over the surface area enclosed by the contour. Finally, from Ohm's law

$$\vec{J} = \sigma (\vec{E} + \vec{v} \times \vec{B}) \quad (\text{A.4})$$

where \vec{v} represents the velocity of the conductor carrying current density \vec{J} . Thus, along the rails $\vec{v} = 0$, but along the two armatures \vec{v} is given by the armature velocity.

We now substitute Eq. (A.4) into (A.3) and apply the result to a contour that passes along the inner surface of each armature and along the inner surface of the rails. Evaluating the integral in the counterclockwise direction, we easily find

$$\oint \frac{\vec{J}}{\sigma} \cdot d\vec{\ell} - v_1 W_1 B_1 + v_2 W_2 B_2 = - \mu \frac{dj_1}{dt} W_1 (D - x_1) - \mu \frac{dj_2}{dt} W_2 (D - x_2) \quad (\text{A.5})$$

Equation (A.5) can be written

$$\oint \frac{\vec{J}}{\sigma} \cdot d\vec{\ell} + \frac{\partial}{\partial t} (L_1) = 0 \quad (\text{A.6})$$

where L is, according to the standard definition, given by

$$L = \frac{1}{i} \int_S \vec{B} \cdot d\vec{A} = \frac{\mu}{h_1} W_1 (D - x_1) + \frac{\mu}{h_2} W_2 (x_2 - D) \quad . \quad (A.7)$$

It is then apparent that Eq. (A.6) is just Eq. (2.4), written in terms of dimensional variables, provided

$$\oint \frac{\vec{J}}{\sigma} \cdot d\vec{\ell} = iR \quad . \quad (A.8)$$

We now use the additional Maxwell equation

$$\mu \vec{J} = \vec{\nabla} \times \vec{B} \quad , \quad (A.9)$$

and the elementary expression for the resistance of a conductor of length ℓ_0 ,

$$R = \frac{1}{\sigma} \int_0^{\ell_0} \frac{dx}{h\delta(x)} \quad . \quad (A.10)$$

Here h represents the conductor height and δ the thickness or extent to which the current has penetrated beneath the surface. It is assumed that δ may vary with position. Equations (A.9) and (A.10) are now substituted into Eq. (A.8) and the integrals performed along the IRG rails, the RG rails, and each of the armatures. If the resulting expression is inspected, it becomes readily apparent that the two sides of (A.8) are equal if δ is given on each surface by

$$\delta = \frac{-B_S}{[\vec{\nabla} \vec{B} \cdot \hat{n}]_S} \quad . \quad (A.11)$$

In Eq. (A.11), \hat{n} represents the unit normal to the surface (pointing into the conductor), and the subscript S denotes that the quantity is to be evaluated at the surface of the conductor in question.

As an application of Eq. (A.11) consider the simple case of constant current and calculate δ for the upper rail in the IRG. For this case an exact analytic expression exists for the induction field inside the conductor ($y > 0$),⁶ viz.,

$$B(y,t) = \mu j_1 \operatorname{Erfc}\left(\sqrt{\frac{\mu \sigma}{4t}} y\right) \quad (A.12)$$

where Erfc is the complementary error function given by

⁶Powell, J.D., "Thermal-Energy Transfer from Arc to Rails in an Arc-Driven Railgun," IEEE Trans. Magn. MAG-20, 395 (1984). See also Ballistic Research Laboratory Report No. ARBRL-TR-02530, October 1983.

$$\operatorname{Erfc}(r_0) = \frac{2}{\sqrt{\pi}} \int_{r_0}^{\infty} e^{-r^2} dr . \quad (\text{A.13})$$

If we now note that $\hat{n} = \hat{a}_y$, differentiate (A.12), and substitute into (A.11) we obtain

$$\delta = \left(\frac{\pi t}{\mu \sigma} \right)^{\frac{1}{2}} . \quad (\text{A.14})$$

Equation (A.14) is the standard expression for constant-current skin depth.

DISTRIBUTION LIST

<u>No. of Copies</u>	<u>Organization</u>	<u>No. of Copies</u>	<u>Organization</u>
2	Administrator Defense Technical Info Center ATTN: DTIC-FDAC Cameron Station, Bldg 5 Alexandria, VA 22304-6145	1	Commander US Army Materiel Command ATTN: AMCDRA-ST 5001 Eisenhower Avenue Alexandria, VA 22333-0001
10	DIR/DB/Standard GE47 HQ Washington, DC 20505	1	Commander US Army Missile Command R&D Center ATTN: AMSMI-R Redstone Arsenal, AL 35898
1	HQDA ATTN: DAMA-ART-M Washington, DC 20310	2	Commander US AMCCOM ARDEC CCAC Benet Weapons Laboratory ATTN: SMCAR-CCB-TL SMCAR-LCB-DS (Dr. C.A. Andrade) Watervliet, NY 12189-4050
1	Commander USA LABCOM ATTN: ALSMLC-TD (Joe Spellman) 2800 Powder Mill RD Adelphi, MD 20783-1145	1	Commander US Army Armament, Munitions & Chemical Command ATTN: AMSMC-IMP-L Rock Island, IL 61299-7300
1	Commander Armament RD&E Center US Army AMCCOM ATTN: SMCAR-MSI Dover, NJ 07801-5001	1	Commander US Army Aviation Systems Command ATTN: AMSAV-ES 1200 Goodfellow Blvd. St. Louis, MO 63120
1	Commander Armament RD&E Center US Army ARDEC ATTN: SMCAR-TDC Dover, NJ 07801	1	Director US Army Aviation Research & Technology Center Ames Research Center Moffett Field, CA 94035-1099
1	Commander Armament R&D Center US Army AMCCOM ATTN: SMCAR-SCA-E (Mr. H. Kahn) Dover, NJ 07801-5001	2	Commander US Army Communications - Electronics Command ATTN: AMSEL-ED AMSEL-IM-L, B (Reports Section) 2700 Ft. Monmouth, NJ 07703-5000
1	Commander Armament R&D Center ATTN: DRDAR-LCA-C (Dr. Thaddeus Gora) Dover, NJ 07801-5001		

DISTRIBUTION LIST

<u>No. of</u> <u>Copies</u>	<u>Organization</u>	<u>No. of</u> <u>Copies</u>	<u>Organization</u>
2	Director US Army Missile & Space Intelligence Center ATTN: AMSMI-YDL Redstone Arsenal, AL 35898-5500	2	Commander Naval Research Laboratory ATTN: Dr. I.M. Vitkovitsky, Code 4701 Mr.R. Ford, Code 4474 Washington, DC 20375
1	Director Ballistic Missile Defense Advanced Technology Center ATTN: BMDATC-M (Dr. D.B. Harmon) PO Box 1500 Huntsville, AL 35807	1	AFWL/SUL Kirtland AFB, NM 87117
1	Director DARPA ATTN: Dr. Peter Kemmey 1400 Wilson Blvd. Arlington, VA 22209	5	Air Force Armament Laboratory ATTN: AFATL/DLODL AFATL/DLJG, (Mr. K. Cobb) AFATL/DLYS, (CPT J. Brown) AFATL/DLYS, (LT J. Martin) AFATL/DLYS, (Dr. T. Aden) Eglin AFB, FL 32542-5000
1	Commander US Army Tank Automotive Command ATTN: AMSTA-TSL Warren, MI 48397-5000	1	AFAPL/POOS-2 ATTN: Dr. Charles E. Oberly Wright-Patterson AFB Dayton, OH 45433
1	Commandant US Army Infantry School ATTN: ATSH-CD-CSO-OR Ft. Benning, GA 98433-5000	1	Director Brookhaven National Laboratory ATTN: Dr. J.R. Powell, Bldg 129 Upton, NY 11973
2	Commander SDIO ATTN: SDIO/KEW (BG M. O'Neil) SDIO/IST (Dr. D. Duston) Washington, DC 30201-7100	1	Director Lawrence Livermore National Lab ATTN: Dr. R.S. Hawke, L-156 PO Box 808 Livermore, CA 94550
1	Director US Army Research Office ATTN: Dr. Mikael Ciftan Research Triangle Park, NC 27709-2211	4	Director Los Alamos National Laboratory ATTN: MSG 787, (Mr. Max Fowler) Dr. J.V. Parker Dr. William Condit MS D472, (Dr. Mark Parsons) Los Alamos, NM 87545
1	Commander Naval Surface Weapons Center ATTN: Mr. P.T. Adams, Code G-35 Dahlgren, VA 22448	1	Sandia National Laboratory ATTN: Dr. Maynard Cowan, Dept 1220 PO Box 5800 Albuquerque, NM 87185

DISTRIBUTION LIST

<u>No. of</u> <u>Copies</u>	<u>Organization</u>	<u>No. of</u> <u>Copies</u>	<u>Organization</u>
1	Astron Research & Engineering ATTN: Mr. Charles Powars 2028 Old Middlefield Way Mountain View, CA 94043	1	General Dynamics ATTN: Dr. Jaime Cuadros PO Box 2507 Pomona, CA 91766
2	Austin Research Associates ATTN: Dr. Millard L. Sloan Dr. William E. Drummond 1091 Rutland Drive Austin, TX 87858	1	General Electric Company ATTN: Dr. John Hickey, Bldg 37, Room 380 1 River RD Schenectady, NY 12345
3	Maxwell Laboratories ATTN: Dr. Rolf Dethlefsen Dr. Michael M. Holland Dr. Mark Wilkinson 8888 Balboa Avenue San Diego, CA 92123	2	General Electric Company (AEPD) ATTN: Dr. William Bird Dr. Slade L. Carr RD#3, Plains RD Ballston Spa, NY 12020
3	Electromagnetic Research, Inc. ATTN: Dr. Henry Kolm Dr. Peter Mongeau Mr. William Snow 625 Putnam Avenue Cambridge, MA 62139	1	General Research Corporation ATTN: Dr. William Isbell 5383 Hallister Avenue Santa Barbara, CA 93111
1	BDM Corporation ATTN: Dr. David Elkin 20160 Old Columbia RD Columbia, MD 21046	1	Gould Defense Systems, Inc. Ocean Systems Division ATTN: Dr. Donald M. McEligot One Corporate Place Newport Corporate Park Middleton, RI 02840
1	Boeing Aerospace Company ATTN: Dr. J.E. Shrader PO Box 3999 Seattle, WA 98134	2	IAP Research, Inc. ATTN: Dr. John P. Barber Mr. David P. Bauer 7546 McEwen RD Dayton, OH 45459
2	GA Technologies, Inc. ATTN: Dr. Robert Borque Dr. L. Holland PO Box 85608 San Diego, CA 92138	1	LTV Aerospace & Defense Company ATTN: Dr. Michael M. Tower Dr. C.H. Haight, MS TH-83 PO Box 650003 Dallas, TX 75265-0003
2	GT Devices ATTN: Dr. Shyke Goldstein Dr. Y.C. Thio 5705-A General Washington Drive Alexandria, VA 22312	1	Pacific-Sierra Research Corp. ATTN: Dr. Gene E. McClellan 1401 Wilson Blvd. Arlington, VA 22209

DISTRIBUTION LIST

<u>No. of Copies</u>	<u>Organization</u>	<u>No. of Copies</u>	<u>Organization</u>
2	Physics International Company ATTN: Dr. A.L. Brooks Dr. Frank Davies 2700 Merced Street San Leandro, CA 94577	1	Texas Technical University Department of EE/Computer Science ATTN: Dr. M. Kristiansen Lubbock, TX 79409-4439
1	R&D Associates ATTN: Dr. Peter Turchi PO Box 9695 Marina del Rey, CA 90291	1	Tuskegee Institute Dept. of Mechanical Engineering ATTN: Dr. Pradosh Ray Alabama 36088
1	Rockwell International Rocketdyne Division ATTN: Dr. Earl Deder, MS HE14 6633 Canoga Avenue Canoga Park, CA 91304	1	University of Alabama in Huntsville School of Science & Engineering ATTN: Dr. C.H. Chen Huntsville, AL 35899
3	SAIC ATTN: Dr. Jad H. Batten Dr. G. Rolader Mr. L. Thornhill 1503 Johnson Ferry RD, Suite 100 Marietta, GA 30062	1	University of Miami ATTN: Dr. Manuel A. Huerta Physics Department PO Box 248046 Coral Gables, FL 33124
1	System Planning Corporation ATTN: Donald E. Shaw 1500 Wilson Blvd. Arlington, VA 22209	1	University of Tennessee Space Inst. ATTN: Dr. Dennis Keefer Tullahoma, TN 37388-8897
1	Westinghouse Electric Corporation Marine Division ATTN: Dr. Dan Omry Dr. Ian R. McNab 401 E. Hendy Avenue Sunnyvale, CA 94088-3499	3	University of Texas Center for Electromechanics Balcones Research Center ATTN: Mr. William Weldon Mr. Raymond Zaworka Dr. Harry Fair 10100 Burnet RD, Bldg 133 Austin, TX 78758
			<u>Aberdeen Proving Ground</u>
1	Westinghouse R&D Laboratory ATTN: Dr. Bruce Swanson 1310 Beulah RD Pittsburgh, PA 15233		Dir, USAMSAA ATTN: AMXSY-D AMXSY-MP, H. Cohen
2	Auburn University ATTN: Dr. Raymond F. Askew, Dir., Leach Nucl Sci Cntr Dr. E.J. Clothiaux, Dept. of Physics Alabama 36849-3501		Cdr, USATECOM ATTN: AMSTE-SI-F Cdr, CRDC, AMCCOM ATTN: SMCCR-RSP-A SMCCR-MU SMCCR-SPS-IL